Journal of Materials Chemistry A

Accepted Manuscript

ROYAL SOCIETY OF CHEMISTRY

www.rsc.org/materialsA

Journal of Materials Chemistry A

ARTICLE

Co-electrolysis of H_2O and CO_2 in a solid oxide electrolysis cell with hierarchically structured porous electrodes

Received 00th January 20xx,
Accepted 00th January 20xx

DOI: 10.1039/x0xx00000x

www.rsc.org/

Chenghao Yang,[a] Jiao Li[a], James Newkirk[b], Valerie Baish[b], Renzong Hu[c], Yu Chen[d] and Fanglin Chen[d]

Solid oxide electrolysis cell with novel asymmetric-porous structured electrodes have been fabricated by the combination of freeze-drying tape-casting and impregnation method. The electrodes possess unique channel-like pores with nano- or sub-micro-sized catalysts homogenously coated on the inner face of porous scaffold. The straight channel-like pores in the electrodes facilitate mass transport while the nano- or sub-micro-sized catalysts promote the electrode electrochemical reactions. The cell demonstrates low electrode polarization resistance values of 0.27, 0.19 and 0.14 Ω cm^2 at OCV in 50 vol.% H_2O-25 vol.% H_2-25 vol.% CO_2 at 800, 850 and 950°C, respectively. The cell DC voltage-current density dependence is generally linear at all temperatures, and high current densities of 0.8, 1.1 and 1.66 A cm^{-2} for 50 vol.% H_2O-25 vol.% H_2-25 vol.% CO_2 co-electrolysis have been obtained with 1.30 V applied voltage at 800, 850 and 900°C, respectively. Compared to that of the cell fabricated by conventional or phase-inversion method, the mass transportation limitation phenomenon in the porous electrodes is mitigated and cell performance is greatly improved.

1. Introduction

Currently, heavy dependence on limited fossil fuels has highlighted energy and environmental concerns. The fabrication of hydrogen (H_2) through H_2O electrolysis or non-fossil synthetic gas (syngas, CO+H_2) through CO_2-H_2O co-electrolysis by solid oxide electrolysis cell (SOEC) technology has attracted many interests, due to its high efficiency and clean characters [1-3]. Especially, syngas is the raw material for synthetic hydrocarbon fuels by Fisher-Tropsch process [4-6]. It has the promise to make a new paradigm for energy storage and CO_2 sequestration, since CO_2 can be captured from atmosphere or recycled from fossil fuel energy systems [7]. Also, SOECs can take advantage of the heat and electrical power supplied by next generation nuclear plant and other renewable energy sources, such as wind, solar and geothermal energy et al., for H_2O electrolysis and CO_2-H_2O co-electrolysis, offering an efficient option for large scale hydrogen or syngas generation.

Strontium doped lanthanum manganite (LSM)-yttria-stabilized zirconia (YSZ) composite has been used as the conventional SOEC oxygen electrode material [8, 9]. In LSM-YSZ oxygen electrode, LSM provides electrochemical activity for oxygen evolution reaction (OER) and electronic conductivity, while YSZ provides ionic conductivity and improves the adhesion between the LSM-YSZ and the YSZ electrolyte. The development of high efficient SOECs requires to minimize the ohmic losses mainly coming from the electrolyte and polarization losses mainly coming from the electrodes. However, the traditional screen-printing method has difficulty in achieving an uniform LSM-YSZ composition and an efficient connection between the LSM-YSZ oxygen electrode and the YSZ electrolyte, the cell performance is limited [10, 11]. An infiltration method has been utilized by us to coat the nano- or sub-micro-sized LSM particles into the porous YSZ substrate to fabricate the SOEC oxygen electrode. Since the OER sites are either near the LSM/YSZ/gas three-phase boundaries (TPBs) or on the surface of the dense LSM rafts, the OER sites in the infiltrated LSM-YSZ oxygen electrode can be greatly enlarged, and the cell performance is significantly advanced [12]. However, a mass transportation limitation phenomenon has been observed when the cell was operated at a relative high current density, particularly in electrolysis mode, which is ascribed to that the reactant gas (RG) in the cell electrode functional layer is not sufficient for electrode electrochemical reaction (Fig. S4). Later, a phase-inversion method has been utilized to optimize the microstructure of Ni-YSZ hydrogen electrode [13]. The fabricated hydrogen electrode possesses an unique two-layer structure, a thin small finger-like porous layer serves as the hydrogen electrode functional layer adjacent to the electrolyte where electrochemical reactions take place, and a thick porous layer with large finger-like pores provides effective reactant gases delivery to and/or from the electrode functional layer. Polarization study of the electrolysis cell demonstrates that the mass transportation limitation was mitigated by employing this unique structured hydrogen electrode (Fig. S6).

Herein, to further mitigate the mass transportation limitation in both hydrogen electrode and oxygen electrode of the single cell, tri-layer YSZ(porous)/YSZ(dense)/YSZ(porous) lamination has been prepared by a freezing-drying tape-casting method. Similarly, the fabricated asymmetric porous YSZ scaffold has a thin layer with small channel-like pores and a thick porous layer with large channel-like pores. Then, the Ni-samarium doped ceria (SDC) catalyst and LSM-SDC catalysts have been loaded into the porous YSZ layers by an impregnation method, to prepare the Ni-SDC-YSZ hydrogen electrode and LSM-SDC-YSZ oxygen electrode, respectively. The electrodes microstructure and its effects on the electrode electrochemical performances of the fabricated single cells have been systemically analyzed and studied.

2. Experimental

Ni-SDC-YSZ/YSZ/LSM-SDC-YSZ symmetric porous structured SOECs were used for the high temperature electrolysis and co-electrolysis test. The symmetric porous YSZ(porous)/YSZ(dense)/YSZ(porous) architecture was

[a] New Energy Research Institute, School of Environment and Energy, South China University of Technology, Guangzhou Higher Education Mega Center, Guangzhou, Guangdong 510006, China.
Email: esyangc@scut.edu.cn
[b] ENrG Inc. 155 Rano Street, Suite 300, Buffalo, NY 14207, USA.
[c] School of Materials Science and Engineering, South China University of Technology, Guangzhou 510640, PR China
[d] Department of Mechanical Engineering, University of South Carolina, 300 Main Street, Columbia, SC 29208, USA.
† Electronic Supplementary Information (ESI) available. See DOI: 10.1039/x0xx00000x

fabricated by freeze-drying tape-casting technology [14-16]. The freeze-drying tape-casting apparatus is similar to the that reported by Sofie et al. [14]. Aqueous YSZ electrode slurry and YSZ electrolyte slurry with solid loading of 25 vol.% and 15 vol.%, respectively, were prepared with an ammonium polyacrylate dispersant (Darvan C-N, R.T. Vanderbilt Co., Inc., Norwalk, CT), a thickener (Vanzan, R.T. Vanderbilt Co., Inc., Norwalk, CT), and an acrylic latex emulsion binder system (Duramax HA-12, Rohm & Haas, Philadelphia, PA). Firstly, the aqueous YSZ electrode slurry with 25% solid loading was cast using a 8 in. doctor blade assembly. After frozen for half an hour, the YSZ electrolyte slurry was directly deposited on the YSZ electrode substrate by air-brushing method. YSZ electrolyte substrate was then laminated onto the YSZ electrode substrate surface. The symmetric YSZ electrode substrate/YSZ electrolyte substrate/YSZ electrode substrate skeleton tri-layers were then co-fired at 1450°C for 12 h, to obtain the symmetric YSZ(porous)/YSZ(dense)/YSZ(porous) architecture. Then, the Ni-SDC-YSZ hydrogen electrode and LSM-SDC-YSZ oxygen electrode were prepared by impregnation method. Aqueous solution of $La(NO_3)\cdot 6H_2O$ (Alfa Aesar, ACS 99.9%), $Sr(NO_3)_2$ (Alfa Aesar, ACS 99.9%), $Mn(NO_3)_2\cdot 4H_2O$ (Alfa Aesar, ACS 99.9%) to yield a composition of $(La_{0.75}Sr_{0.25})_{0.95}MnO_3$ (LSM), and $Ni(NO_3)_2\cdot 4H_2O$ (Alfa Aesar, ACS 99.9%) to yield NiO, were infiltrated into each porous YSZ matrix, respectively. Then, the cell was followed by drying at 200°C and decomposition of the nitrite at 800°C. After several impregnating, drying and firing steps, and the cell was finally fired at 850°C to form NiO and perovskite phase LSM crystals, as described in the literature [17]. Then, the NiO-YSZ hydrogen electrode and LSM-YSZ oxygen electrode were impregnated by a 3 mol/l $Sm_{0.2}Ce_{0.8}(NO_3)_x$ solution. The impregnation and calcination process were repeated for several cycles to achieve ~10 wt % $Sm_{0.2}Ce_{0.8}O_2$ (SDC) in the NiO-YSZ and LSM-YSZ electrodes, respectively. The prepared SOEC button cells have an effective cathode area of 0.35 cm^2.

Platinum current collectors were formed by printing platinum paste on the surfaces of the electrodes, and then fired at 1000°C for 0.5 h. A glass-ceramic bonding/sealing material (Aremco-552 high temperature ceramic adhesive paste) was used to seal the button cell to an alumina tube. The high temperature electrolysis cell testing system is assembled according to the schematic diagram shown in Fig. 1, as we described previously [10]. High temperature electrolysis testing system includes major components such as gas supply, delivery and control elements (gas cylinders, pressure regulators and mass flow controllers), steam generation and monitoring elements (humidifier and humidity sensors), temperature measurement, high temperature furnace, solid oxide electrolysis button cells, and electrochemical testing equipment (potentiostat/galvanostat and impedance response analyzers). Hydrogen and carbon dioxide flow rates were controlled by a precision mass flow controller (APEX, Alicat Scientific, U.S.). Hydrogen and carbon dioxide mixture was mixed with water vapor using a humidifier. The amount of water vapor in the gas mixture was continuously measured in term of absolute humidity (AH, the vol.% of humidity in the total gas volume) using an on-line humidity sensor (Vaisala Model HMP 337). The current density-voltage curves as well as the impedance spectra were measured with a four probe method using a multi-channel VersaSTAT (Princeton Applied Research). The cross-sectional microstructure of the tested cell was characterized using a scanning electron microscopy (SEM) (FEI Quanta 200 ESEM).

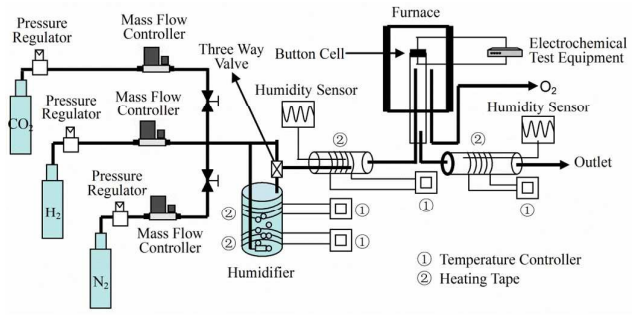

Fig. 1. Schematic of experimental setup for high temperature co-electrolysis cell measurements.

3. Results and discussion

Fig. 2 shows cross-sectional SEM images of Ni-SDC-YSZ/YSZ/LSM-SDC-YSZ SOEC fabricated by free-drying tape casting combined with infiltration method. The obtained SOEC button cell has ~0.1 cm Ni-SDC-YSZ hydrogen electrode layer, ~130 μm YSZ membrane electrolyte, and ~0.1 cm LSM-SDC-YSZ oxygen electrode layer. As indicated in Fig. 2(A), the YSZ electrolyte is dense without pores, the symmetric porous hydrogen and oxygen electrode layers are well attached to the dense YSZ electrolyte membrane. The straight tubular pores and YSZ scaffold are homogenously mixed together in porous electrodes, in which the big tubular pores serve as fuel delivery channels. The amount *Q* (moles/sec) of the reactant gas (RG) transported to the electrode functional layer per unit time in the porous media can be defined by the Fick's Equation [18, 19],

$$Q_1 = -D_{RG}^{eff} A \frac{dC}{dx} \quad (1)$$

where D_{RG}^{eff} (cm^2 s^{-1}) is the RG effective diffusivity coefficient, A (cm^2) is the diffusion area, $\frac{dC}{dx}$ (mol cm^{-1}) is the concentration gradient between the porous electrode surface and functional layer. But in SOEC porous electrodes, the gas molecules tend to be impeded by the pore walls due to the complex structure and tortuosity of the porous electrode, therefore, the gas diffusion flux should be corrected to account for the effects of such blockage, which can be accomplished by employing a modified or effective diffusivity:

$$D_{RG}^{eff} = D_{RG} \frac{\varepsilon}{\tau} \quad (2)$$

where D_{RG} (cm^2 s^{-1}) is the RG diffusion coefficient, ε is the electrode porosity, τ is the tortuosity of the porous electrode. Under steady-state conditions, Equation (1) can be written as follows:

$$Q_1 = -D_{RG} \frac{\varepsilon}{\tau} A \frac{c_{RG}^* - c_{RG}^0}{\delta} \quad (3)$$

where δ (cm) is the thickness of porous electrode, c_{RG}^* (mol L^{-1}) is the concentration of RG in porous electrode functional layer, c_{RG}^0 (mol L^{-1}) is the bulk steam concentration, respectively. When the SOEC is operated for electrolysis or co-electrolysis, the SOEC need to sustain a certain value of current density. It is interesting to consider the situation that the RG concentration in electrode functional layer drops to zero, which represents the limiting case for mass transport in porous electrode. A higher applied current density to the SOEC than that which causes the RG concentration to fall to zero would be utilized for generating heat loss other than for electrolysis or co-electrolysis. We call this current density as the limiting current density of the SOEC. According to the Faraday's law, amount Q_2 (mole s^{-1}) of the RG per unit time in the functional layer for electrolysis or co-electrolysis at limiting applied current density j_L (A cm^{-2}) can be expressed as follows:

$$Q_2 = \frac{j_L A}{nF} \quad (4)$$

where n is the number of the electrons involved in the charge transfer reaction and F (C mol^{-1}) is the Faraday's constant. A limiting current density condition can be expressed as following:

$$Q_1 = Q_2 \quad (5)$$

and the limiting current density can be calculated from Equation (3), (4) and (5) by setting $c_{RG}^* = 0$ or $P_{RG}^* = 0$:

$$j_L = -nFD_{RG} \frac{\varepsilon}{\tau} \frac{c_{RG}^0}{\delta} \quad (6)$$

We can see that the effective diffusivity and limiting current density are proportional to the reciprocal of square of the geometrical tortuosity. It is expected that the unique channel-like porous microstructure produced in this study will provide efficient fuel gas delivery through the electrode support layer to the electrode functional layer while facilitating the reaction

product removal from the electrode functional layer to the large channel-like porous support layer. The gas diffusion resistance from the hydrogen electrode ($R_{Diffusion\,(HE)}$) (Ω cm^2) and oxygen electrode ($R_{Diffusion\,(OE)}$) (Ω cm^2) can be estimated by the following equations [20, 21]:

$$R_{Diffusion\,(HE)} = \left(\frac{RT}{2F}\right)^2 \delta_{HE} \frac{1}{D_{RG}} \frac{\tau_{HE}}{\varepsilon_{HE}} \left(\frac{1}{P_{H_2}} + \frac{1}{P_{RG}}\right) \times (1.0133 \times 10^5 \frac{Pa}{atm})^{-1} \quad (7)$$

$$R_{Diffusion\,(OE)} = \left(\frac{RT}{4F}\right)^2 \delta_{OE} \frac{1}{D_{O2,N_2}} \frac{\tau_{OE}}{\varepsilon_{OE}} \left(\frac{1}{P_{O_2}} - 1\right) \times (1.0133 \times 10^5 \frac{Pa}{atm})^{-1} \quad (8)$$

where R (J mol^{-1} K^{-1}) is the universal gas constant, T (K) is the temperature, D_{H2O,H_2} (cm^2 s^{-1}) is the binary diffusivity for a mixture of H_2O and H_2, D_{O2,N_2} (cm^2 s^{-1}) is the binary diffusivity for a mixture of O_2 and N_2, P_{H_2} and P_{H_2O} (atm) represent the H_2 and steam partial pressure in hydrogen electrode reaction area, P_{O_2} (atm) represents the O_2 partial pressure in oxygen electrode reaction area, respectively. As expected, the diffusion resistances for the hydrogen electrode and oxygen electrode will decrease with the low tortuosity factor ~1.3 and high porosity ~50 vol.% of both the hydrogen electrode and oxygen electrode as shown in Fig. 2. According to the Equation (7) and (8), the diffusion resistances for the hydrogen electrode and oxygen electrode under open circuit voltage (OCV) condition in 50 vol.% H_2O-50 vol.% H_2 atmosphere have been calculated to be 0.0055 and 0.0031 Ω cm^2 at 800°C (D_{H_2O,H_2}= 3.966 cm^2 s^{-1}, D_{O_2,N_2}= 0.959 cm^2 s^{-1}), respectively. Also, the limiting current density would increase due to the low tortuosity factor and high porosity of both the electrodes. The calculation results based on H_2O-H_2 provides a baseline for comparison, and is much similar to that reported previously for steam electrolysis [10, 12]. Thus, we can come to the conclusion that the gas diffusion resistances in the porous electrode would be greatly reduced and the j_L of the electrodes would be greatly enhanced by employing the unique asymmetric porous structured electrodes fabricated by the combination of freeze drying tape casting and infiltration method. But, when CO_2 was introduced into the feeding gas, a slight increase of the hydrogen electrode diffusion resistance has been observed and it increases with the increasing CO_2 concentration. It is because that the lower gas diffusion coefficient of CO_2 rich reactant gas, since the molecular weight of CO_2 is much higher than that of H_2O.

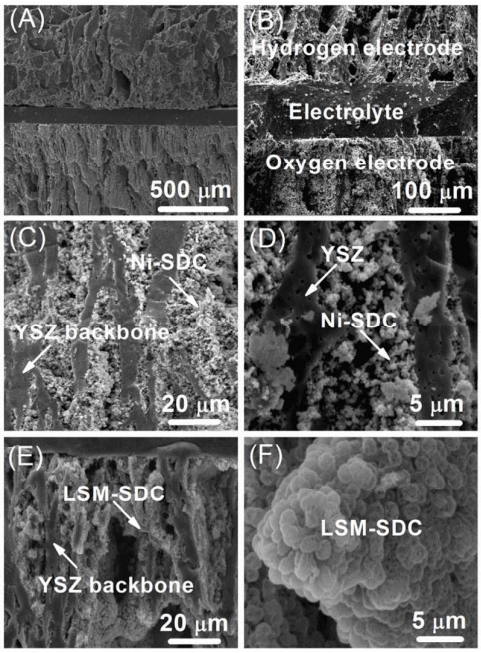

Fig. 2. (A, B) Cross-sectional SEM image of the Ni-SDC-YSZ/YSZ/LSM-SDC-YSZ solid oxide electrolysis cell (SOEC) fabricated by freeze-drying tape casting and infiltration method, (C) SEM and (D) high magnification SEM micrograph of the Ni-SDC infiltrated YSZ hydrogen electrode, (E) SEM and (F) high magnification SEM image of the LSM-SDC infiltrated YSZ oxygen electrode.

Fig. 2(B) indicates that the dense YSZ electrolyte and porous YSZ electrodes backbones have been bonded firmly together by the co-sintering process. The YSZ scaffold can be utilized as bridges between the electrodes and electrolyte for oxygen ions transportation, which can greatly reduce the fuel electrode and electrolyte interfacial resistance. Also, compared to that of the SOEC with electrodes prepared by printing method [10], it can efficiently prevent the delaminating of porous electrodes from the dense YSZ electrolyte in high humidity atmosphere at high temperature and. Fig. 2 (C, D) present the Ni-SDC infiltrated YSZ hydrogen electrode, the nano- or sub-micro-sized Ni-SDC particles are homogenously coated on inner face of the porous YSZ scaffold, and form as the thin function layer on the surface of the YSZ backbone. Ni is an excellent catalyst with good electronic conductivity, SDC is a mixed electronic/ionic conductor and YSZ is a good ionic conductor, therefore, the hydrogen electrode reaction kinetics can be further promoted by extending reaction sites not only at the Ni/YSZ(SDC)/gas TPBs but also at the nano- or sub-micro-sized mixed ionic/electronic conductor SDC rafts. Similar effect has been found in the oxygen electrode, SEM images of the LSM-SDC-YSZ oxygen electrode are shown in Fig. 2 (E, F), the nano or sub-micro-sized LSM-SDC particles are homogenously coated on inner face of the porous YSZ scaffold. The mathematic simulation and experimental results indicate that the hydrogen electrode reaction sites for hydrogen or syngas fabrication and oxygen electrode reaction sites for OER can be further improved by extend the TPB width in atomic dimensions, respectively [12, 22].

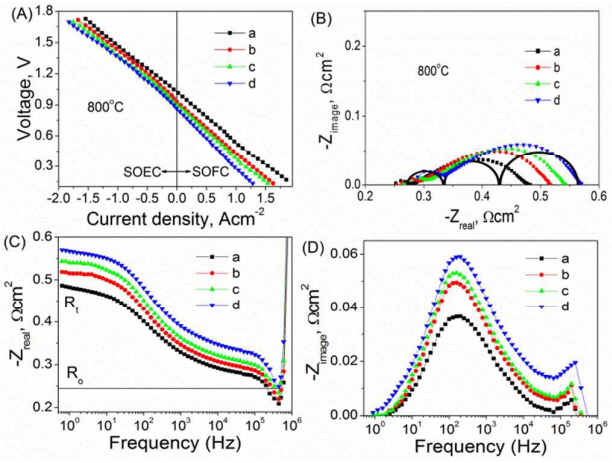

Fig. 3. DC potential-current density curves (A), impedance spectra ((B) complex plane, and (C, D) Bode presentations) of the Ni-SDC-YSZ/YSZ/LSM-SDC-YSZ SOEC fabricated by freeze-drying tape casting and infiltration method operated under SOEC and SOFC modes at 800°C with (a) 50 vol.% H_2-50 vol.% H_2O, (b) 37.5% H_2-50 vol.% H_2O-12.5% CO_2, (c) 25% H_2-50 vol.% H_2O-25% CO_2 and (d) 50 vol.% H_2O-12.5% H_2-37.5% CO_2 as feeding gases.

Fig. 3A show the polarization characters of the single cell fabricated by the combination of freeze-drying tape casting and infiltration method. Polarization study of the cell has been conducted with potential as function of current densities (v-*j* curves) in both solid oxide fuel cell (SOFC) and SOEC modes at 800°C, and four different gas compositions were used as feeding gas, e.g. 50 vol.% H_2-50 vol.% H_2O, 37.5 vol.% H_2-50 vol.% H_2O-12.5 vol.% CO_2, 25 vol.% H_2-50 vol.% H_2O-25 vol.% CO_2, and 12.5 vol.% H_2-50 vol.% H_2O-37.5 vol.% CO_2. Positive current densities indicate power generation (SOFC mode), while negative current densities indicate power consumption (SOEC mode). Cell potential values at zero current density correspond to the OCV. As presented in the figure, the cell OCV is influenced by the H_2O-CO_2 to hydrogen ratio, and it decreases when the H_2O-CO_2 to hydrogen ratio increases, as predicted for these gas compositions from the Nernst Equation [23, 24]. In both SOFC and SOEC modes, the voltage varies linearly with the increasing current density. For comparison, the traditional single cell with

Ni-YSZ hydrogen electrode, YSZ electrolyte and LSM-YSZ oxygen electrode fabricated by dry-pressing, dip-coating and screen printing method, respectively, has also been studied in the similar testing condition (Fig. S1) [10]. When 50 vol.% H_2O-50 vol.% H_2 was used as feeding gas, the current density of the cell fabricated by the traditional method was only 0.30 A cm^{-2} under 1.3 applied voltage (Fig. S2). For the single cell with similar configuration but LSM-SDC-YSZ oxygen electrode fabricated by infiltration method (Fig. S3), the cell performance was greatly enhanced. But it is noticed that the cell voltage is linearly with the cell current density at low current density, the cell voltage begins to increase rapidly at relatively high current density due to the diffusion limitation (Figure S4) [12]. When a phase-inversion method was used to fabricate the hydrogen electrode [13], it was observed that the mass transport limitation was mitigated (Figure S5 and Figure S6). However, the voltage of the cell fabricated by freeze-drying tape-casting and infiltration method keeps almost linearly with cell current density in 50 vol.% AH-50 vol.% H_2. Comparison with that of the cells fabricated by traditional methods as indicated in Fig. S1, Fig. S3 and Fig. S5, the mass transport limitation related to the gas diffusion resistance is further mitigated by employing this unique structured electrodes fabricated by the combination of freeze-drying tape-casting and infiltration method (Fig. 3A), which is well consistent with cell microstructure analysis. The cell exhibits an advanced performance for H_2O electrolysis, and a cell current density of 0.65 A cm^{-2} has been obtained under 1.30 V applied electrolysis voltage. It is much higher than that of the cell fabricated by traditional dry-pressing and infiltration method, which demonstrates a current density of 0.51 A cm^{-2} under 1.30 V applied voltage in 50 vol.% AH-50 vol.% H_2 as indicated in Fig. S7. Moreover, the YSZ electrolyte thickness of anode supports as indicated in Fig. S1, Fig. S3 and Fig. S5 are only 10-30 μm, while it is ~130 μm in the present work. It indicates the single cell performance can be improved by employing a thinner YSZ electrolyte. Further, compared with the single cells fabricated with traditional dry-pressing, dip-coating and infiltration method, the single cell reported here are much easier for fabrication and mass production. Moreover, as interpreted in Equation 2, the gas diffusion coefficients are closely related to the gas compositions. When the gas contains more CO_2, the diffusion limitation is more obvious than the H_2-H_2O system, as indicated in Fig. S2, Fig. S4 and Fig. S6. The single cell fabricated by freeing-drying tape-casting method has also been utilized for H_2O-CO_2 co-electrolysis. The cell exhibits a much higher performance for H_2O-CO_2 co-electrolysis than that of H_2O electrolysis. The cell co-electrolysis current density increases with the increasing CO_2 content, as indicated in Fig. 3A. It is well known that the kinetics and diffusion are slow for CO_2 electrolysis and H_2O-CO_2 co-electrolysis. To accelerate the slow reaction and diffusion, the continuous supply of sufficient oxygen-containing reactants is needed. The increase molar ratio of CO_2 to H_2O can provide more primary reactant via water-gas-shift (WGS), enhance the thermo-electrochemical reaction kinetics, and promote the H_2O/CO_2 electrolysis and H_2O-CO_2 co-electrolysis [25].

Electrochemical impedance spectra of the Ni-SDC-YSZ/YSZ/LSM-SDC-YSZ SOEC fabricated by the combination of freeze-drying tape-casting and infiltration method have been examined at 800°C and OCV with 50 % H_2O - (50% H_2, 37.5% H_2-12.5% CO_2, and 12.5% H_2-37.5% CO_2). The cell impedance spectra as well as the Bode presentations (real and imaginary parts as function of the frequency) are shown in Fig. 3B, C and D. The cell impedance spectra were evaluated by fitting impedance data with the equivalent circuit. As presented in Fig. 3B, three arcs at high-, middle- and low-frequency range are observed in the impedance spectra, respectively. The three arcs are most likely associated with at least two electrode processes for the electrode electrolysis and co-electrolysis reaction, respectively. The high-frequency (1 kHz-100 kHz) and middle-frequency (10 Hz-1 kHz) arcs are associated to the polarization during charge transfer or gas diffusion process in the electrodes, the low-frequency (0.1 Hz-10 Hz) arc is associated to the gas-phase and ionic diffusion [26]. In the impedance spectra as indicated Fig. 3B, the intercepts of the impedance arcs with the real axis at high and low frequencies represent cell ohmic resistance (R_o) and total resistance (R_t), respectively, while the intercept on the real impedance axis between high and low frequency is related the polarization resistance (R_p). The R_o mainly comes from the electrolyte, electrode/electrolyte contact and lead wires, and the R_p includes considerable contribution coming from the electrodes. The cell ohmic resistance (R_o) is ~0.25 Ω cm^2 and almost does not change, but the cell R_p increases from 0.2 Ω cm^2 to 0.23, 0.25 and 0.27 Ω cm^2 when the CO_2 concentration in the gas mixture increases from 0 to 12.5%, 25% and 37.5%, respectively. It is much smaller than that of the cell with similar compositions and fabricated by traditional methods. With 50 % H_2O-50 % H_2 as feeding gas, the R_p of the cell fabricated by traditional dry pressing and screening printing method is about 1.09 Ω cm^2 [10], that of the cell fabricated by dry pressing and infiltration method is 0.48 Ω cm^2 [12], and that of the cell fabricated by phase-inversion and infiltration method is 0.45 Ω cm^2 [13]. Also, the experimental results indicates the R_p increment occurs reproducibly upon the increasing concentration of CO_2 in the reactant gas flowing. As interpreted previously, the cell demonstrates a slight slower the CO-CO_2 oxidation/reduction process than that of the H_2-H_2O.

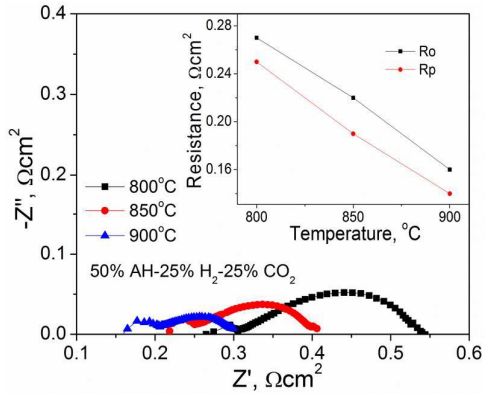

Fig. 4. Impedance spectra for Ni-SDC-YSZ/YSZ/LSM-SDC-YSZ SOEC measured at OCV in 50 vol.% H_2O-25 vol.% H_2-25 vol.% CO_2 at 800, 850 and 900°C, respectively. Inset in Fig. 4 shows the ohmic resistance (Ro) and polarization resistance (Rp) of the cell at different temperatures.

Fig. 4 shows the impedance spectra of the fabricated cell measured in 50 vol.% H_2O-25 vol.% H_2-25 vol.% CO_2 gas mixture at 800, 850 and 900°C, respectively. As observed from the figure, most of the total cell impedance comes from the electrodes. It is ascribed to the contribution of the YSZ bridges connected between YSZ matrices in the oxygen and hydrogen electrodes to YSZ electrolyte formed during the freeze-drying tape-casting and co-sintering process, which benefits the transportation of O^{2-} from the hydrogen electrode to the oxygen electrode. Therefore, the oxygen electrode/electrolyte interfacial resistance as well as the R_o is greatly reduced. The cell electrode polarization losses decrease obviously with the increasing of cell operating temperature, and the cell electrode R_p values are 0.27, 0.19 and 0.14 Ω cm^2 at 800, 850 and 900°C, respectively.

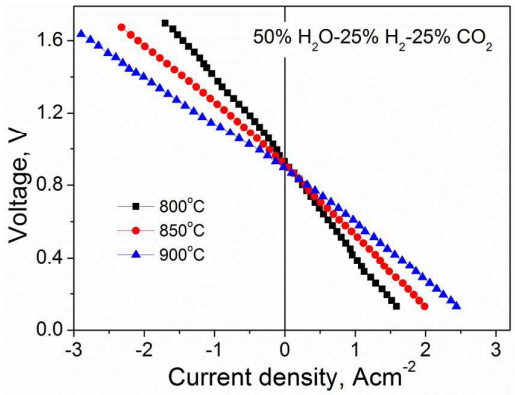

Fig. 5. DC potential-current density curves of Ni-SDC-YSZ/YSZ/LSM-SDC-YSZ SOEC recorded under SOEC and SOFC modes in 50 vol.% H_2O-25% H_2-25% CO_2 at 800, 850 and 950°C, respectively.

Fig. 5 shows the DC potential-current density curves of the cell recorded under SOEC and SOFC modes in 50 vol.% H_2O-25 vol.% H_2-25 vol.% CO_2 at 800, 850 and 950°C, respectively. The cell OCV ranges from 0.86 to 0.90 V, which are consistent with the values predicted using the Nernst equation. It can be seen that the DC voltage-current density dependence is generally linear at all temperatures. The current density values at a given applied voltage generally increased with increasing temperature, as that of the previous high temperature steam electrolysis [10, 12]. High co-electrolysis current densities of 0.8, 1.1 and 1.66 A cm^{-2} with 1.30 V applied voltage at 800, 850 and 900 °C, respectively.

After initial performance tests of the fabricated cell, the durability test for H_2O-CO_2 co-electrolysis has been conducted. As indicated in Fig. S8, the voltage of Ni-SDC-YSZ/YSZ/LSM-SDC-YSZ single cell fabricated by Freeze-drying Tape-casting and infiltration method was recorded under a co-electrolysis current density load of 0.33 A cm^{-2} for over 120 h in 50 vol.% H_2O-25 vol.% CO_2-25 vol.% H_2 at 800°C. The cell voltage required to maintain a 0.33 A cm^{-2} co-electrolysis current density is plotted as a function of the operating time. The cell voltage increased and then leveled off after ~10 h under the co-electrolysis mode. The increase in the cell electrode polarization resistance is probably ascribed to responsible for the rise of the cell voltage [12]. The cell was partially activated during the recording of the DC voltage-current density curves, and the electrode polarization resistance was affected by the application of current, but the impedance of the cell returned to the initial state after ~10 h co-electrolysis test. It indicates the SOEC with unique hierarchically structured porous electrodes fabricated by Freeze-drying Tape-casting and infiltration method is promising for high efficient H_2O electrolysis and H_2O-CO_2 co-electrolysis.

4. Conclusions

SOEC with novel asymmetric-porous structured electrodes has been fabricated by the combination of freeze-drying tape-casting and impregnation method. The unique structured porous electrodes with large channel-like pores provide effective reactant gases delivery to and/or from the electrode functional layer, and the mass transportation limitation phenomenon in the cell porous electrodes is greatly mitigated. The cell demonstrates low electrode polarization resistance values of 0.27, 0.19 and 0.14 Ω cm^2 at OCV in 50% H_2O-25% H_2-25% CO_2 at 800, 850 and 950°C, respectively. The cell DC voltage-current density dependence is generally linear at all temperatures, and high current densities of 0.8, 1.1 and 1.66 A cm^{-2} for in 50% H_2O-25% H_2-25% CO_2 co-electrolysis with 1.30 V applied voltage at 800, 850 and 900°C, respectively. The experimental results demonstrate that SOEC with unique hierarchically structured porous electrodes fabricated by Freeze-drying Tape-casting and infiltration method is promising for high efficient H_2O electrolysis and H_2O-CO_2 co-electrolysis.

Acknowledgements

We gratefully acknowledge the financial support from Natural Science Foundation of China (51402109), Natural Science Foundation of Guangdong Province, China (S2013010014883), Scientific Research Foundation for the Returned Overseas Chinese Scholars, State Education Ministry ((2013)1792), and Fundamental Research Funds for Central Universities, China (2013ZM051).

Notes and references

1 Z. L. Zhan, W. Kobsiriphat, J. R. Wilson, M. Pillai, I. Kim and S. A. Barnett, *Energ. Fuel*, 2009, **23** , 3089-3096.
2 Q. X. Fu, C. Mabilat, M. Zahid, A. Brisse and L. Gautier, *Energy Environ. Sci.*, 2010, **3**, 1382-1397.
3 A. Hauch, S. D. Ebbesen, S. H. Jensen and M. Mogensen, *J. Mater. Chem.*, 2008, **18**, 2331-2340.
4 D. J. Wilhelm, D.R Simbeck, A.D. Karp and R. L. Dickenson, *Fuel Process. Technol.*, 2001, **71**, 139-148.
5 S. N. Naik, V. V. Goud, P. K. Rout and A. K. Dalai, *Renew. Sust. Energ. Rev.*, 2010, **14**, 578-597.
6 U. M. Graham, A. Dozier,R. A. Khatri, M. C. Bahome, L. L. Jewell, S. D. Mhlanga, N. J. Coville, and B. H. Davis, *Catal. Lett.*, 2009, **129**, 39-45.
7. C. M. Stoots, J. E. O'Brien and J. J. Hartvigsen, *Int. J. Hydrogen Energy*, 2009, **34**, 4208-4215.
8 F. H. Heuveln and H. J. M. Bouwmeester, *J. Electrochem. Soc.*, 1997, **144**, 134-140.
9 A. Brisse, J. Schefold and M. Zahid, *Int. J. Hydrogen Energy*, 2008, **33**, 5375-5382.
10 C. H. Yang, A. Coffin and F. L. Chen, *Int. J. Hydrogen Energy*, 2010, **35**, 3221-3226.
11. M. D. Liang, B. Yu, M. F. Wen, J. Chen, J. M. Xu and Y. C. Zhai, *J. Power Sources*, 2009, **190**, 341-345.
12. C. H. Yang, C. Jin, A. Coffin and F. L. Chen, *Int. J. Hydrogen Energy*, 2010, **35**, 5187-5193.
13. C. H. Yang, C. Jin and F. L. Chen, *Electrochim. Acta*, 2010, 56, 80-84.
14. S. W. Sofiew, *J. Am. Ceram. Soc.*, 2007, **90**, 2024-2031.
15. Y. Chen, Q. Liu, Z. B. Yang, F. L. Chen, M. F. Han, *RSC Adv.*, 2012, **2**, 12118-12121.
16. Y. Chen, Y. Lin, Y. X. Zhang, S. W. Wang, D. Su, Z. B. Yang, M. F. Han, F. L. Chen, *Nano Energy* 2014, **8**, 25-33.
17. W. S. Wang, Y. Y. Huang, S. Jung, J. M. Vohs and R. J. Gorte, *J. Electrochem. Soc.*, 2006, **153**, A2066-A2070.
18. R. P. O'Hayre, S. W. Cha, W. Colella and F. B. Prinz. *Fuel cell fundamentals*. 2nd ed. John Wiley & Sons, Inc., 2008.
19. C. H. Yang, C. Ren, L. Yu and C. Jin, *Int. J. Hydrogen Energy*, 2013, **38**, 15348-15353.
20. A. Leonide, V. Sonn, A. Weber and E. Ivers-Tiffée, *J. Electrochem. Soc.*, 2008, **155**, B36-B41.
21. Y. Chen, Y. Lin, Y. X. Zhang, S. W. Wang, D. Su, Z. B. Yang, M. F. Han and F. L. Chen, *Nano Energy*, 2014, **8**, 25-33.
22. J. M. Vohs and R. J. Gorte, *Adv. Mater.*, 2009, **21**, 943-956.
23J. E. O'Brein, C. M. Stoots, J. S. Herring, P. A. Lessing, J. J. Hartvigsen and S. Elangovan, *J. Fuel Cell Sci. Tech.*, 2005, **2**, 156-163.
24. J. E. O'Brein, C. M. Stoots, J. S. Herring and J. J. Hartvigsen, *J. Fuel Cell Sci. Tech.*, 2006, **3**, 213-219.
25. S. Kim, H. Kim, K. J. Yoon, J. H. Lee, B. K. Kim, W. Choi, J. H. Lee and J. Hong, *J. Power Sources*, 2015, **280**, 630-639.
26. T. Kato, K. Nozaki, A. Negishi, K. Kato, A. Monma, Y. Kaga, S. Nagata, K. Takano, T. Inagaki, H. Yoshida, K. Hosoi, K. Hoshino, T. Akbay and J. Akikusa, *J. Power Sources*, 2004, **133**, 169-174.

Graphical Abstract

Solid oxide electrolysis cell with novel asymmetric-porous structured electrodes has been fabricated by freeze-drying tape-casting and impregnation method. The straight channel-like pores in the porous electrode facilitate mass transport while the nano- or sub-micro-sized catalysts promote the electrode electrochemical reactions.